Supporting Information

Accessing Ni(0) to Ni(IV) via Nickel-Carbon-Phosphorus Bond Reorganization

Lirong Lin,[a] David S. Tresp,[a] Denis M. Spasyuk,[b] Roger A. Lalancette,[a] and Demyan E. Prokopchuk[a]*

[a]Department of Chemistry, Rutgers University-Newark, 73 Warren Street, Newark, NJ 07102, United States
*Email: demyan.prokopchuk@rutgers.edu

[b]Canadian Light Source, Saskatoon, SK S7N2V3, Canada

Experimental

General Comments

All reactions were carried out under an atmosphere of nitrogen using standard glove box or high vacuum line (Schlenk) techniques unless stated otherwise. All reagents and solvents were stored under inert gas unless stated otherwise. Inert atmosphere reactions and workup protocols used HPLC-grade, inhibitor-free solvents which were dried and degassed over activated alumina using an IT/Inert solvent purification system. Additionally, Tetrahydrofuran (THF), Fluorobenzene (PhF), Toluene, and MeOH were dried over 20% w/v activated 3 Å molecular sieves.[1] Deuterated solvents were subjected to three freeze-pump-thaw cycles and dried over 10% w/v activated 3 Å molecular sieves in a glove box. Elemental analyses were run by CENTC Elemental Analysis Facility (Department of Chemistry, University of Rochester) on a PerkinElmer 2400 Series II Analyzer. Compounds **PCPNiBr**[2] and [Fc][$B(C_6F_5)_4$][3] were prepared using known literature procedures. Commercially purchased electrolyte [$^nBu_4N$][PF_6] (99%) was recrystallized from fluorobenzene/pentane prior to use.

NMR Spectroscopy. Experiments were conducted on a Bruker Avance III HD 500 MHz NMR and Varian Inova 600 MHz NMR spectrometers. Spectra for ^1H and ^{13}C were referenced to their respective residual protio solvent signal,[4] ^{31}P to external 85% H_3PO_4 (0 ppm), ^{19}F to external $C_6H_5CF_3$ (-63.72 ppm). NMR signal assignations were made by routine one- and two-dimensional experiments, including ^1H-^1H COSY, ^1H-^{13}C HSQC, ^1H-^{13}C HMBC and ^1H-^{31}P HMBC spectroscopies. All NMR measurements were carried out at 25 ºC unless otherwise stated.

X-Ray Crystallography. Single crystals of **1** and **2** were selected and mounted using Paratone onto a nylon fiber and cooled to the data collection temperature of 100(2) K with a stream of dry nitrogen gas. X-ray diffraction intensities were collected on a Bruker SMART APEX II CCD Diffractometer using CuKα (1.54178 Å) radiation.

Electrochemistry. Cyclic voltammetry experiments were conducted under N_2 at 295 ± 3 K using a standard three-electrode setup consisting of a 1 mm PEEK-encased glassy carbon working electrode (eDAQ), graphite rod counter electrode, and Ag wire pseudoreference electrode. The working electrode was polished with 0.25 μm diamond polishing paste, lapping oil, and a rayon microcloth pad (Buehler) inside a glove box and thoroughly rinsed with the solvent used in the corresponding experiment. A Gamry Reference 1010B potentiostat and Gamry software were used for data collection and analysis. The uncompensated solution resistance (R_u) was measured for each electrochemical solution and post-iR corrections were applied to all CV traces. All CVs are referenced to the $Fc^{+/0}$ redox couple (0 V).

EPR Spectroscopy. Continuous-wave X-band (9.43795 GHz) EPR spectra were collected using a Bruker EMXPlus EPR spectrometer with a standard high sensitivity X-band resonator. Spectra were recorded at 77 K suspended in a frozen 2-MeTHF glass (ca. 16 mM, freeze quenched reaction) and contained in 4 mm OD quartz tubes. Microwave power was typically 2 mW, the field was swept by 800 G in 71.84 s, modulated at 100 kHz with 1 G amplitude, and a time constant of 10.24 ms was used. EPR spectra were simulated using EasySpin.[5]

DFT Calculations. Calculations were performed with ORCA Version 5.0.3.[6] Geometry optimization and numerical frequency calculations use the meta-GGA TPSS functional with the def2-TZVP[7] basis sets and def2/J[8] auxiliary basis sets (TPSS-D3(BJ)/def2-TZVP). Single point energies were obtained using the hybrid PW6B95[9] functional with def2-QZVPP basis set,[7] RIJK approximation,[10] and def2/JK auxiliary basis sets[11] (PW6B95-D3(BJ)/def2-QZVPP). All calculations include D3 dispersion correction with Becke-Johnson damping and three-body correction (D3BJ ABC).[12, 13] All calculations utilize the SMD solvation model[14] in THF. Full vibrational and thermochemical analyses were performed on optimized structures to obtain solvent-corrected free energies ($G°$)

and enthalpies ($H°$) under standard state conditions. Optimized ground states all have zero imaginary frequencies while transition states have exactly one imaginary frequency. Transition states have exactly one imaginary frequency and were located using the nudged elastic band method[15] (NEB-TS) within the ORCA software package. The final multi-level Gibbs free energy term is calculated by taking the free energy minus the electronic energy at the TPSS-D3(BJ)/def2-TZVP level of theory (**A**) and adding it to the single point energy at the PW6B95-D3(BJ)/def2-QZVPP level of theory (**B**):

$$G_{solv}(\mathbf{B}) = [(G_{solv}(\mathbf{A}) - E_{solv}(\mathbf{A})] + E_{solv}(\mathbf{B})$$

The final multi-level Gibbs free energy term $G_{solv}(\mathbf{B})$ and Cartesian coordinates are provided in an .xyz file as part of the Supporting Information. Redox potentials were computed relative to ferrocenium/ferrocene ($\mathbf{Fc^{+/0}}$, $E°$ = 0.0 V) using a generic isodesmic reaction scheme approach:

$$n\mathbf{Fc}^{+} + n\mathbf{e}^{-} \rightleftharpoons n\mathbf{Fc} \qquad \Delta G_{Fc} = -23.06nE^{0} = 0.0 \text{ kcal/mol}$$

$$[\mathbf{M}]^{x} + n\mathbf{Fc} \rightleftharpoons [\mathbf{M}]^{x-n} + n\mathbf{Fc}^{+} \qquad \Delta G_{rxn}$$

$$[\mathbf{M}]^{x} + n\mathbf{e}^{-} \rightleftharpoons [\mathbf{M}]^{x-n} \qquad \Delta G_{Fc} + \Delta G_{rxn} = -23.06nE^{0}$$

Syntheses

PCPNiPh (1). In the glovebox, **PCPNiBr** (35 mg, 0.050 mmol) was dissolved in 5.0 mL THF in a Schlenk flask, sealed, then connected to a Schlenk line and cooled to -40 ºC. Next, phenyllithium (53 µL, 0.10 mmol, 1.9 mol/L in Bu_2O) was added to the solution dropwise. The cold bath was removed, and the reaction was stirred at room temperature overnight. MeOH (1.0 mL) was added into the solution to quench the reaction and then solvent was removed under vacuum. After washing with MeOH (3.0 mL x 3), the pale-yellow solid was obtained on a medium-pore glass frit. The analytically pure pale-yellow product (34 mg, 98%) was extracted by running through the glass frit with Pentane (8.0 mL) and drying under high vacuum. X-ray-quality crystals of **1** were obtained by a concentrated pentane solution at room temperature. Anal. calcd (%) for $C_{42}H_{66}NiP_2$: C 72.94 H 9.62, N 0.00; found: C 73.33, H 9.56, N 0.00. ^{1}H NMR (500 MHz, C_6D_6): δ 7.77 (br. 2H, H_{Ph}), 7.19 (1H, H_{Ph}), 7.00 (2H, H_{Ph}), 2.50 (d, 2H), 2.29 (s, 1H, CH_{Ad}), 2.21 (s, 1H, CH_{Ad}), 2.16 (d, 2H), 2.01 (d, 2H), 1.93 (m, 2H, PCH_{Cy}) 1.02-1.80 (m, 51H) (1.77 (2H, PCH_{Cy}), 1.64 (2H, PCH_2), 1.47(2H, PCH_2), 1.34 (1H, Ni-CH)) ppm. Buried resonances from 1.77-1.34 were determined via 2D heteronuclear experiments. ^{13}C{^{1}H} NMR (126 MHz, C_6D_6) δ139.0 (C_{Ph}), 125.3 (C_{Ph}), 120.6 (s, C_{Ph}), 69.6 (t, $^{2}J_{CP}$ = 10.5 Hz, CH$_{Ad}$-Ni), 46.4, 45.4 (vt, J_{CP} =8.2 Hz), 43.7 (vt, J_{CP} = 12.0 Hz), 40.6 (vt, J_{CP} = 10.0 Hz, PCH$_2$), 36.7, 34.4 (vt, PCH$_{Cy}$), 33.5(vt, PCH$_{Cy}$ J_{CP} = 10.0 Hz), 32.4, 31.7 (CH$_{Ad}$), 30.5 (CH$_{Ad}$), 30.4, 30.2, 29.4, 29.0, 28.5, 28.0, 27.7, 27.3, 26.8, 23.1, 14.4 ppm. ^{31}P{^{1}H} NMR (202 MHz, C_6D_6): δ 48.8 ppm.

[PCP(η^6-C$_6$H$_5$)Ni][B(C$_6$F$_5$)$_4$]$_2$ (2). In the glovebox, **PCPNiPh** (6.9 mg, 0.010 mmol) was dissolved in 1.0 mL Toluene in a vial. [Fc][B(C_6F_5)$_4$] (17 mg, 0.020 mmol) was suspended in 2.0 mL Toluene and

added to the solution dropwise. The reaction turned deeper yellow and formed a yellow precipitate immediately. After stirring at room temperature overnight, the liquid was discarded. The precipitate was washed by toluene (3.0 mL x 3) and the resulting brown-yellow colored product was obtained by crystallization via PhF/Et_2O vapor diffusion (9.0 mg, 44%) at -30 °C. X-ray-quality crystals of **[PCP(η^6-C_6H_5)Ni][B(C_6F_5)$_4$]$_2$** were obtained by PhF/Et_2O vapor diffusion at -30 °C. Anal. calcd (%) for $C_{90}H_{66}B_2F_{40}NiP_2$: C 52.74, H 3.25, N 0.00; found: C 52.71, H 3.46, N 0.00. ^{1}H NMR (500 MHz, CD_2Cl_2): δ 7.72 (m, 3H, H_{Ph}), 7.64 (m, 1H, H_{Ph}), 6.58 (m, 1H, H_{Ph}), 3.13 (s, 1H, CH_{Ad}-Ni), 2.80 (m, 1H, CH_{Cy}-P$^+$), 2.54 (m, 1H, CH_{Cy}-P$^+$), 2.39 (m, 1H, CH_2-P$^+$), 2.14 (m, 3H), 1.75 (1H, CH_2-P$^+$), 1.17-2.08 (m, 53H) ppm. ^{13}C{^{1}H} NMR (126 MHz, CD_2Cl_2) δ 149.6 (s, B(C_6F_5)$_4$), 147.6 (s, B(C_6F_5)$_4$), 139.7 (s, B(C_6F_5)$_4$), 137.7 (s, B(C_6F_5)$_4$), 135.8 (s, B(C_6F_5)$_4$), 116.8 (d, J_{CP} = 7.6 Hz, C_{Ph}), 115.9 (d, J_{CP} = 7.6 Hz, C_{Ph}), 114.3 (d, J_{CP} = 5.4 Hz, C_{Ph}), 112.4 (d, J_{CP} = 5.6 Hz, C_{Ph}), 110.4 (s, C_{Ph}), 70.2(s, C_{Ad}-Ni), 52.0 (d, $^2J_{CP}$ = 5.5 Hz, quaternary C_{Ad}), 48.0 (d), 45.1 (s), 44.4 (d), 43.4 (d, $^2J_{CP}$ = 5.3 Hz, quaternary C_{Ad}), 40.4, 38.0 (d), 37.0 (d), 36.4 (d, $^1J_{CP}$ = 36.8 Hz, CH$_{Cy}$-P$^+$), 36.0 (s), 35.8 (d, $^1J_{CP}$ = 67.5 Hz, CH$_2$-P$^+$), 34.3 (d, $^1J_{CP}$ = 35.9 Hz, CH$_{Cy}$-P$^+$), 34.1 (s), 30.3 (s), 29.3 (s), 28.8, 28.7, 28.4, 28.3, 27.3, 27.2, 27.0, 26.8, 26.7, 26.1 (s), 25.9 (s), 25.4 (s) ppm. ^{31}P{^{1}H} NMR (202 MHz, CD_2Cl_2): δ 94.2 (P-Ni), 20.4 (P^+) ppm. ^{19}F{^{1}H} NMR (470 MHz, CD_2Cl_2) δ -132.9, -163.3, -167.3 ppm.

In situ Sequential Oxidation-Reduction of 1

In the glovebox, complex **1** (3.4 mg, 4.9 μmol) and [Fc][B(C_6F_5)$_4$] (8.6 mg, 9.9 μmol) were added to a J. Young NMR tube, followed by 0.60 mL THF. The reaction was placed on a rotating stirrer for an hour and ^{31}P NMR spectroscopy indicated that **1** was fully transformed to **2**. Then, Cp*$_2$Cr (3.2 mg, 9.9 μmol) was added to the mixture and **2** was fully converted to **1** as seen by ^{31}P NMR. Finally, Triphenylphosphine (2.4 mg, 9.1 μmol) was added to the J. Young tube as an internal standard and a sealed insert tube with acetone-d6 was placed into the J. Young tube to improve locking/shimming. By measuring the relative integrations of ^{31}P peaks at 48.8 ppm from **1** and -5.2 ppm from PPh_3 in inverse-gated ^{31}P{^{1}H} NMR (NS = 256), the recovered yield of **1** was determined to be 98% from the average of two independent experiments.

Preparation of [PCPNiPh]$^{\bullet+}$ (**1**$^{\bullet+}$)

In the glovebox, **1** (3.4 mg, 4.9 μmol) was dissolved in 0.1 mL 2-MeTHF and transferred to a 4 mm OD quartz tube. The tube was capped with a rubber septum and cooled to -78 °C. Then, [Fc][B(C_6F_5)$_4$] (4.2 mg, 4.9 μmol) in 0.2 mL 2-MeTHF was slowly added to the EPR tube via syringe -78 °C. The tube was shaken to ensure complete reactant mixing and then freeze-quenched in liquid nitrogen. Subsequently, EPR spectroscopic data was collected at 77 K, with **1**$^{\bullet+}$ being the only detectable EPR-active species in solution (see main text for further discussion).

NMR Spectra

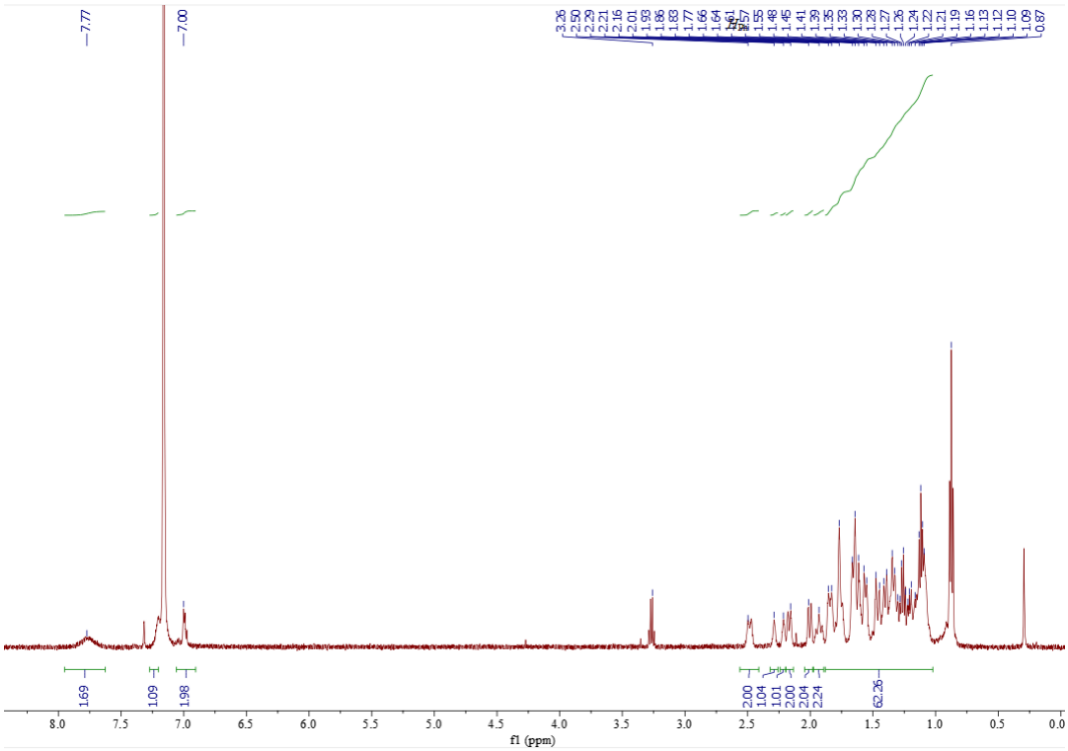

Figure S1 - ^{1}H NMR spectrum of **PCPNiPh** (**1**) (500 MHz, C_6D_6, 25 °C). Peaks at 3.26 and 1.15 ppm are residual Et_2O while peaks at 0.87 and 1.31 ppm are residual pentane.

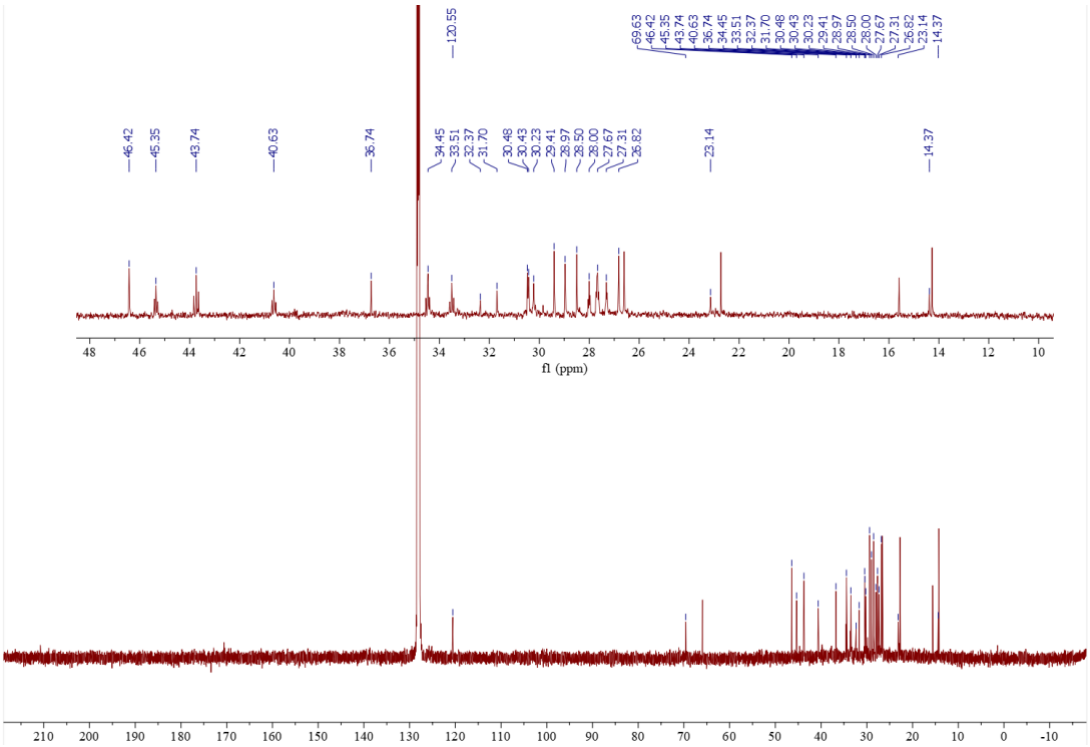

Figure S2 - ^{13}C{^{1}H} NMR spectrum of **PCPNiPh** (**1**) (126 MHz, C_6D_6, 25 °C). Signals at 15.59 and 65.91 ppm are residual Et_2O while signals at 14.27, 22.72 and 34.57 ppm are residual n-pentane. Signals at 139.0 (2C, C_{Ph}), 125.3 (1C, C_{Ph}) are assigned based on ^{1}H-^{13}C HSQC.

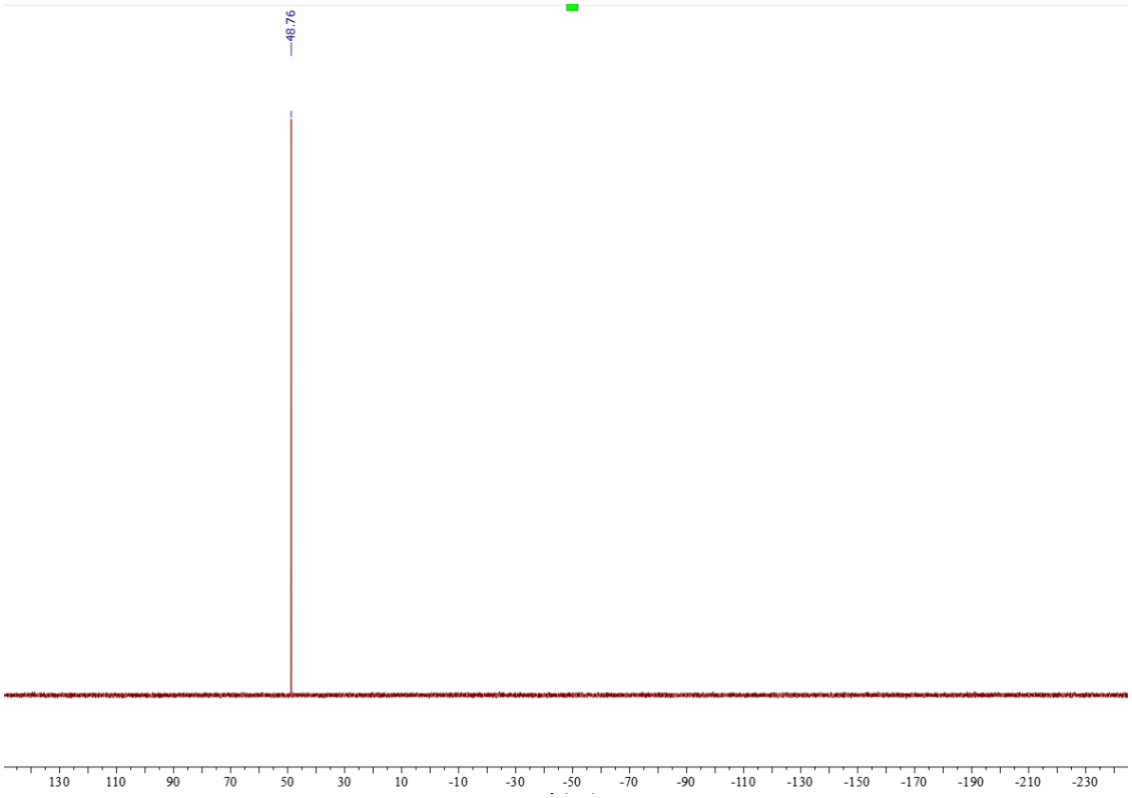

Figure S3 - $^{31}P\{^{1}H\}$ NMR spectrum of **PCPNiPh** (**1**) (202 MHz, C_6D_6, 25 °C).

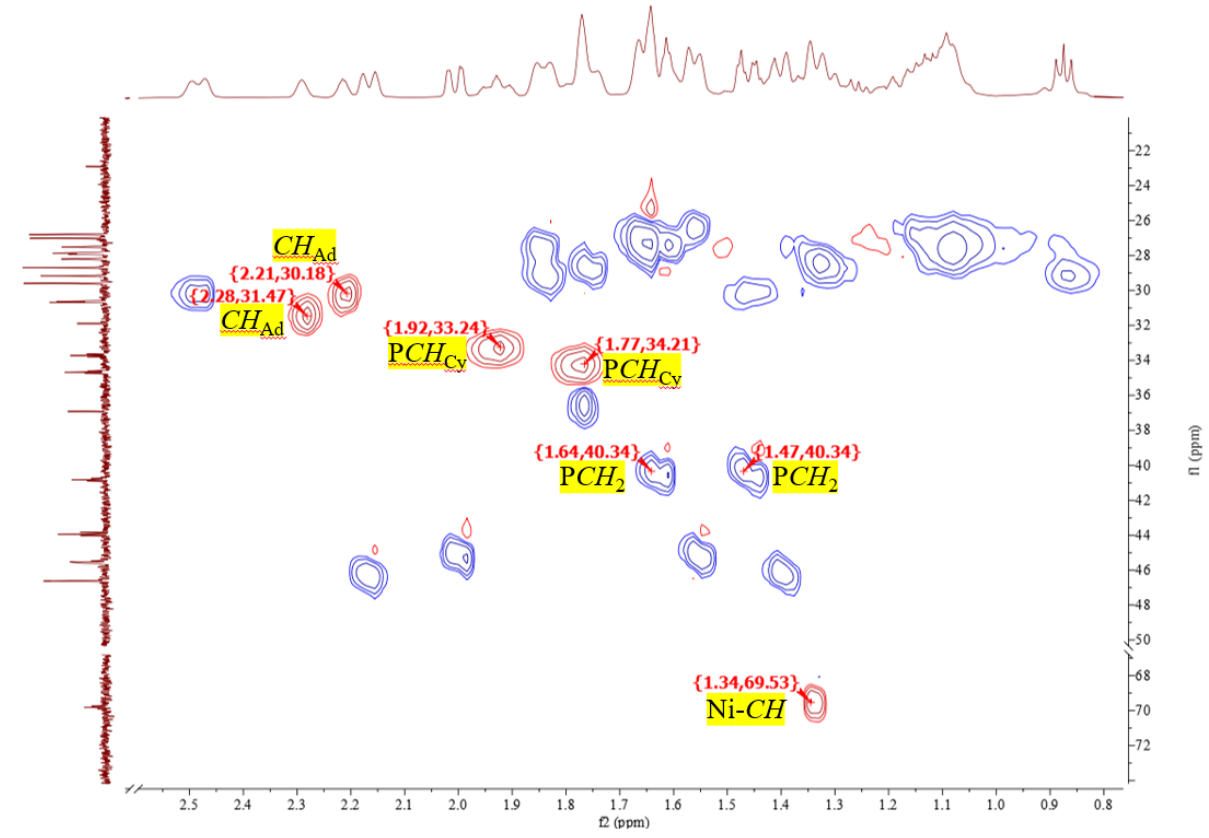

Figure S4 – Multiplicity-edited ^{1}H-^{13}C HSQC NMR spectrum of **PCPNiPh** (**1**) (500, 126 MHz, C_6D_6, 25 °C).

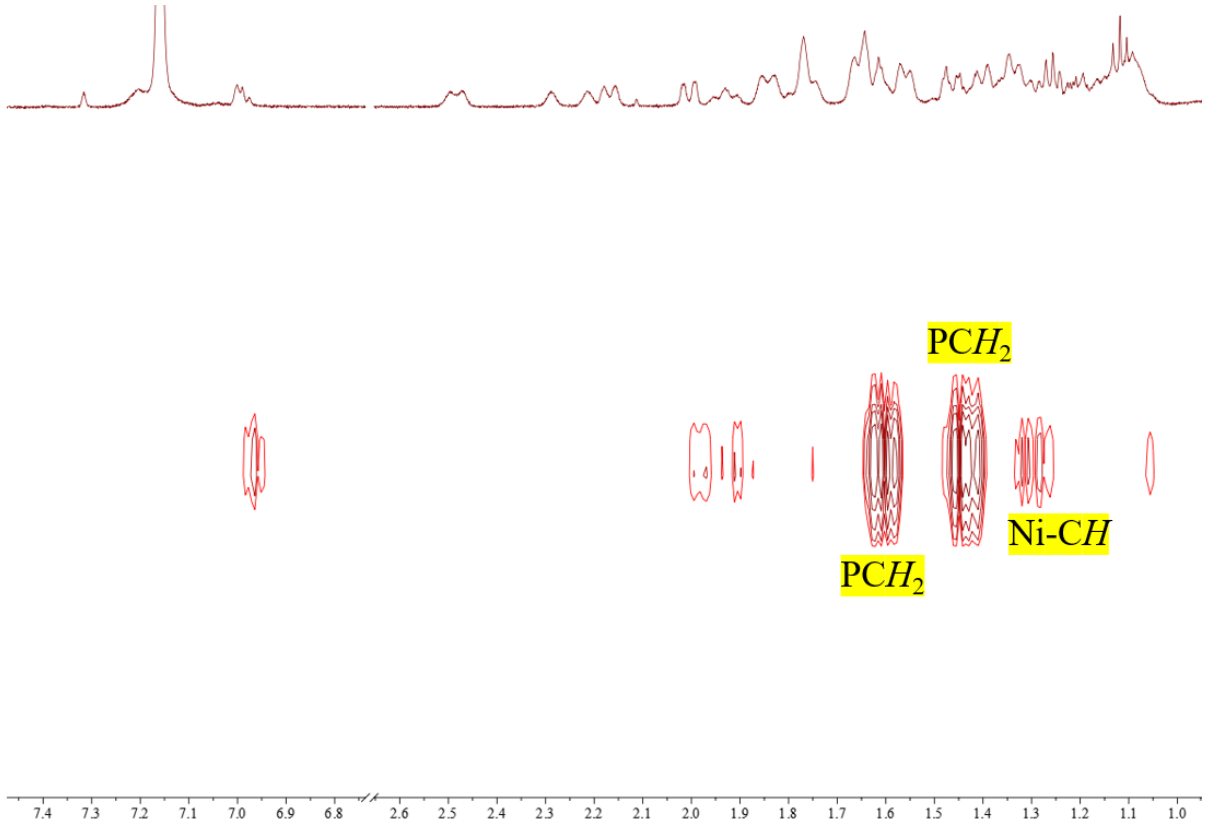

Figure S5 –^{1}H-^{31}P HMBC NMR spectrum of **PCPNiPh** (**1**) (500, 202 MHz, C_6D_6, 25 °C).

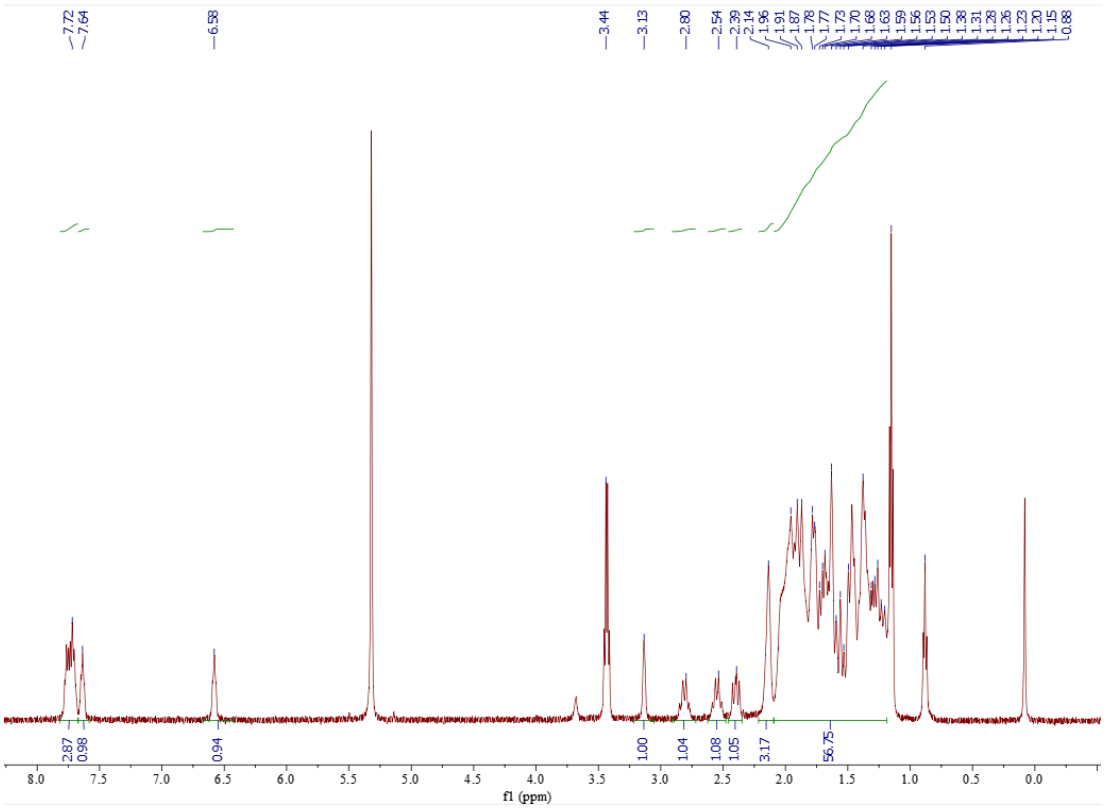

Figure S6 - ^{1}H NMR spectrum of **[PCP(η^{6}-C_6H_5)Ni][B(C_6F_5)$_4$]$_2$** (**2**) (500 MHz, CD_2Cl_2, 25 °C). Multiplets at 3.44 and 1.15 ppm are residual Et_2O while signals at 0.88 and 1.31 ppm are residual pentane.

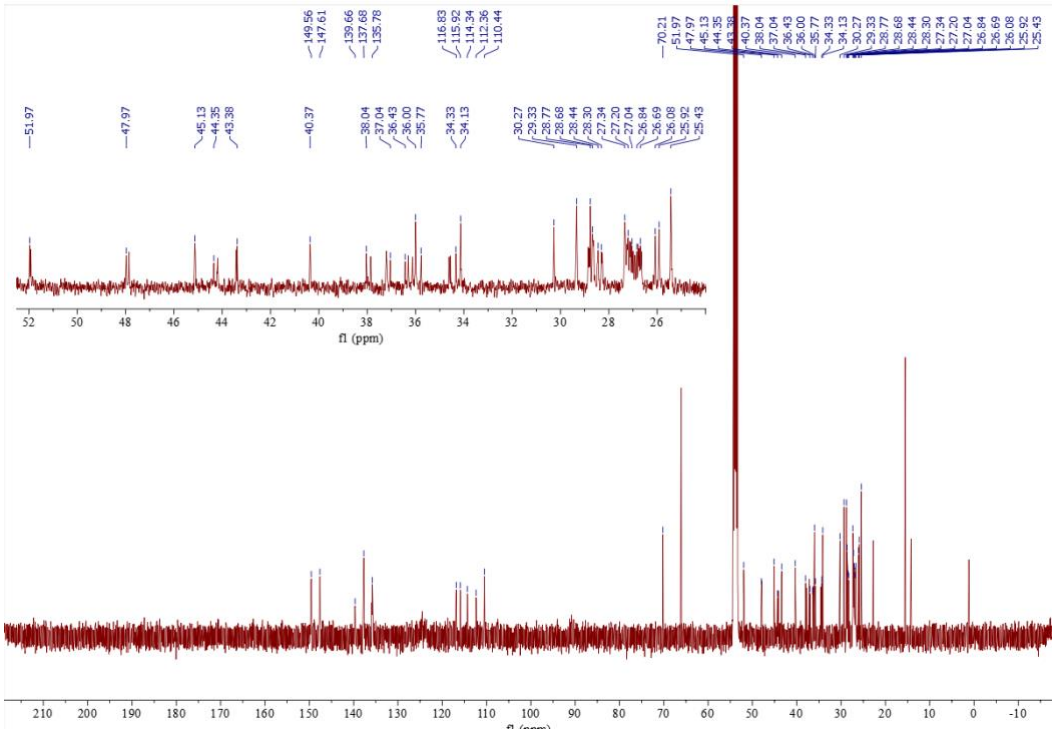

Figure S7 - $^{13}C\{^{1}H\}$ NMR spectrum of **[PCP(η^6-C$_6$H$_5$)Ni][B(C$_6$F$_5$)$_4$]$_2$ (2)** (126 MHz, CD_2Cl_2, 25 °C). Signals at 15.51 and 66.07 ppm are residual Et_2O while signals at 14.22, 22.76 and 34.57 ppm are residual pentane.

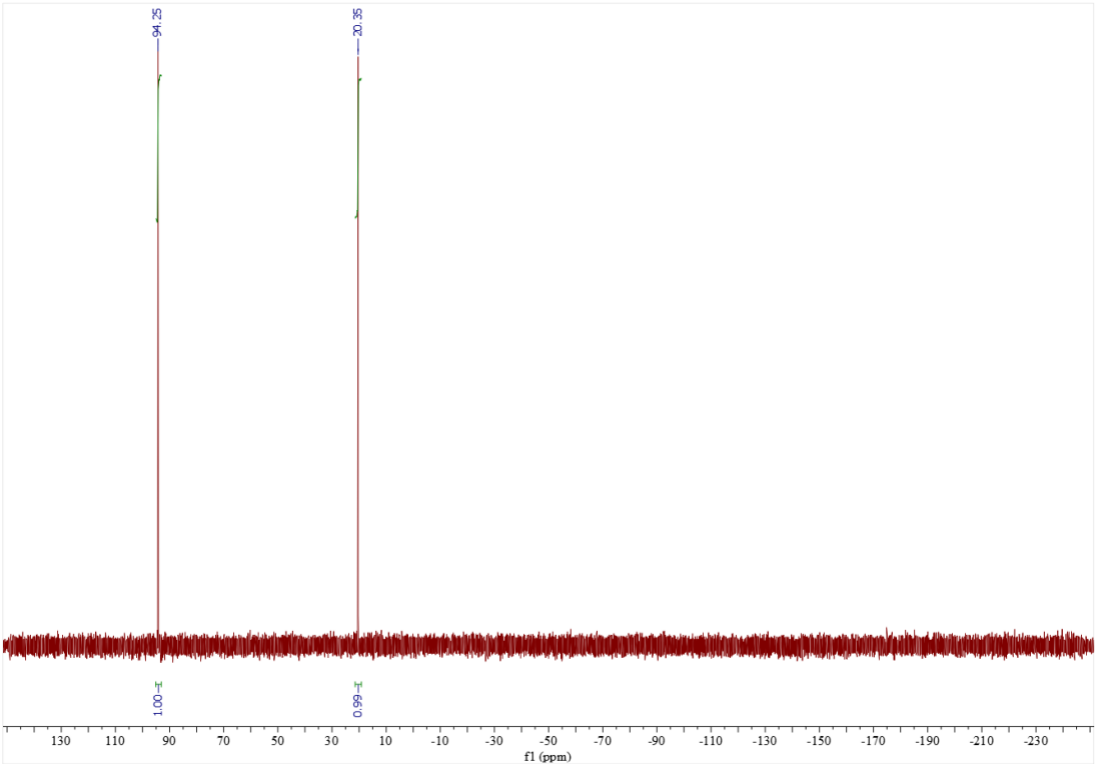

Figure S8 - $^{31}P\{^{1}H\}$ NMR spectrum of **[PCP(η^6-C$_6$H$_5$)Ni][B(C$_6$F$_5$)$_4$]$_2$ (2)** (202 MHz, CD_2Cl_2, 25 °C).

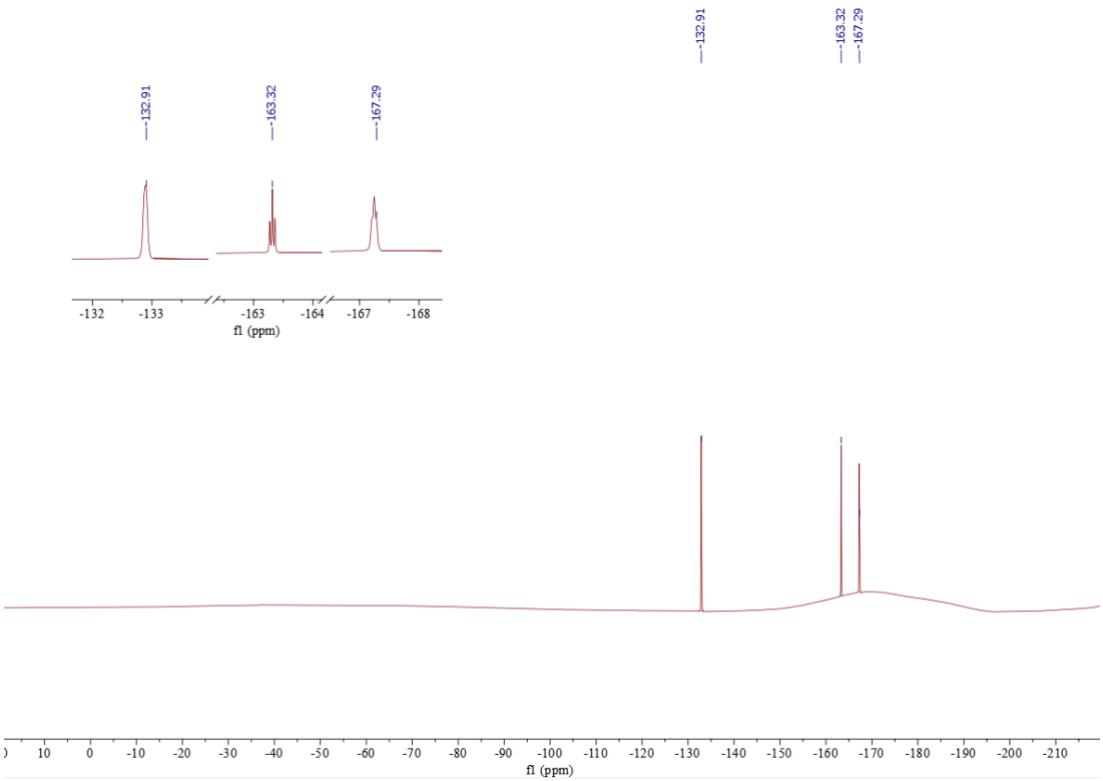

Figure S9 - $^{19}F\{^{1}H\}$ spectrum of **[PCP(η^6-C_6H_5)Ni][B(C_6F_5)$_4$]$_2$ (2)** (470 MHz, CD_2Cl_2, 25 °C)

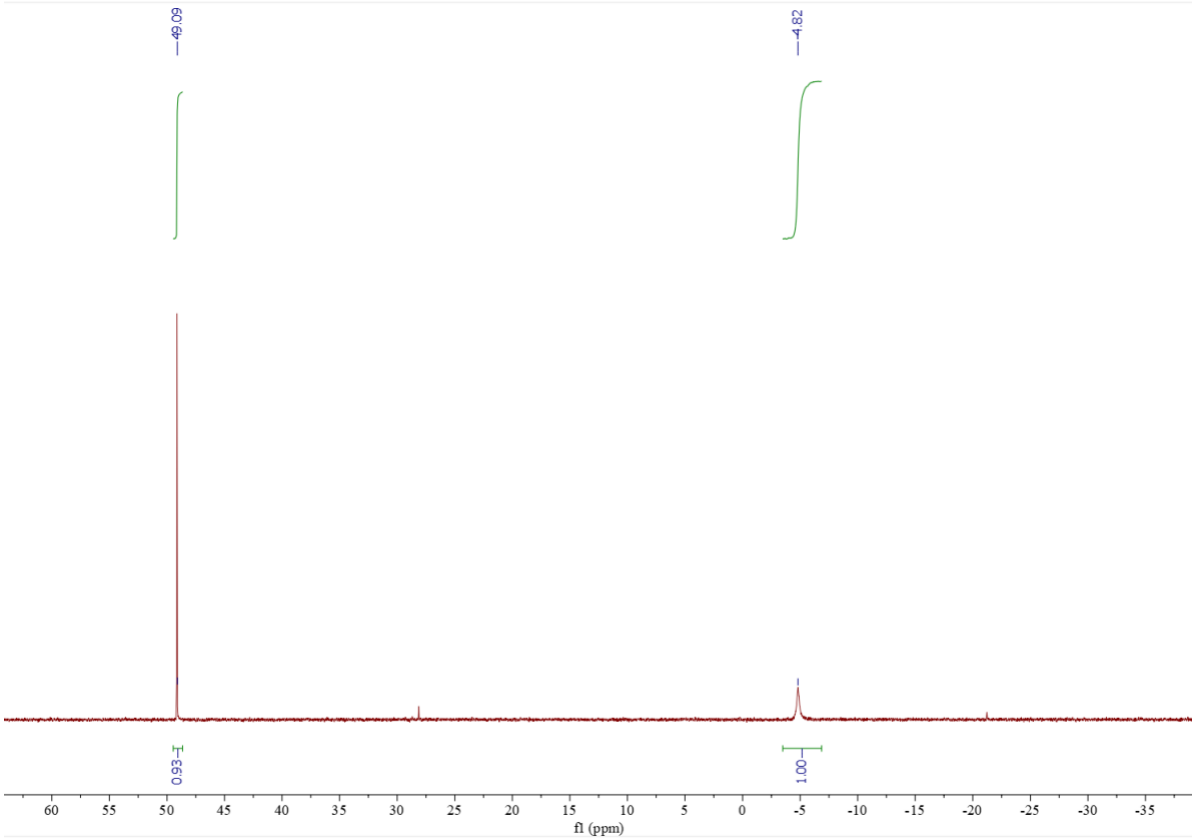

Figure S10 - Inverse-gated $^{31}P\{^{1}H\}$ NMR spectrum of the reaction of **[PCP(η^6-C_6H_5)Ni][B(C_6F_5)$_4$]$_2$ (2)** (12 mg, 0.0059 mmol) with Cp*$_2$Cr (3.8 mg, 0.012 mmol). Triphenylphosphine (3.0 mg, 0.011 mmol) was added as an internal reference (202 MHz, NS = 64, 25 °C).

Electrochemistry

v (mV/s)	I_{pa} (μA)	I_{pc} (μA)	- (I_{pc} / I_{pa})
10	0.371	-0.238	0.64
25	0.454	-0.349	0.77
50	0.604	-0.484	0.80
75	0.753	-0.615	0.82
100	0.877	-0.754	0.86
150	0.997	-0.874	0.88
200	1.197	-0.995	0.83
250	1.304	-1.109	0.85
500	1.692	-1.512	0.89

Table S1. The current response on the cyclic voltammograms of the $Ni^{III/II}$ redox couple for **1** at different scan rates.

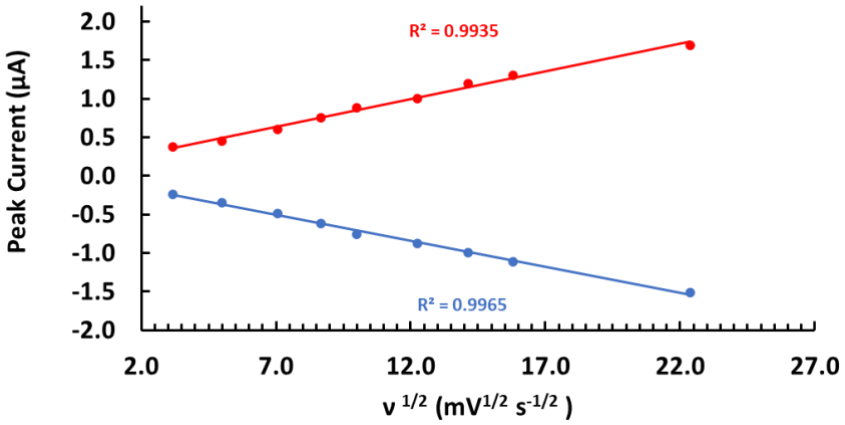

Figure S11. Peak current (μA) vs. the square root of scan rate ($mV^{1/2}$ $s^{-1/2}$) plots of the $Ni^{III/II}$ redox couple for **1**.

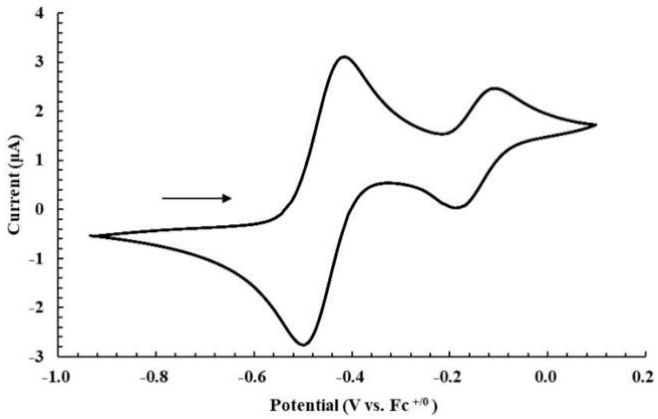

Figure S12. Cyclic voltammograms of the $Ni^{III/II}$ redox couple for **1** with added $FeCp^*_2$ at 50 mV/s. Conditions: N_2, THF, 1 mM analyte, 0.1 M [^{n}Bu$_4$N][PF_6], PEEK-encased glassy carbon working electrode, Type 2 glassy carbon rod counter electrode, Ag/AgCl pseudoreference electrode. Initial scan direction and starting position indicated with a black arrow.

	E_{pa} (mV)	E_{pc} (mV)	ΔE_p (mV)
$FeCp^*_2$	-498.0	-417.0	81
NiPh	-107.1	-184.0	77

Table S2. Peak potential and peak to peak separation of the cyclic voltammograms of **1** at $E_{1/2}$ = -0.14 V and $FeCp^*_2$ in THF. Conditions: 1 mM analyte, 1 mM $FeCp^*_2$, 0.1 M [$^nBu_4N$][PF_6], 50 mV/s.

DFT-Computed Transition State Structures

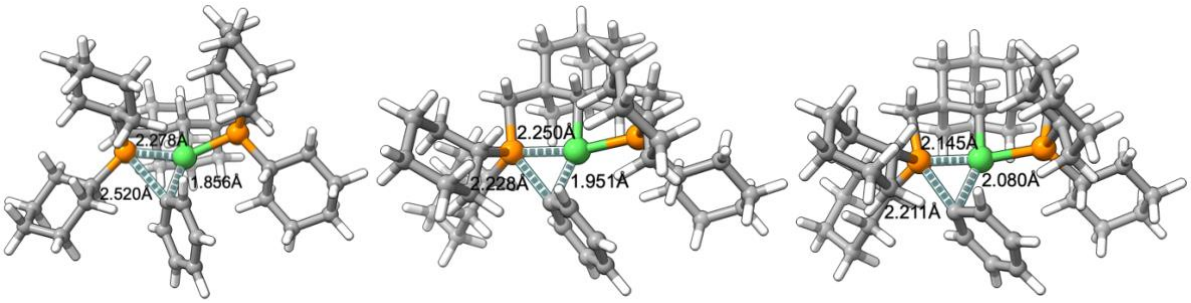

Figure S13. Transition state structures for $\Delta G^{\ddagger}_{A\rightarrow 2}$ (left, 47*i* cm^{-1}) , $\Delta G^{\ddagger}_{1^{\bullet+}\rightarrow B}$ (middle, 143*i* cm^{-1}), and $\Delta G^{\ddagger}_{C\rightarrow 1}$ (right, 124*i* cm^{-1}). Bond distances are provided in Å.

References

1. D. B. G. Williams and M. Lawton, *J. Org. Chem.*, 2010, **75**, 8351.
2. L. Lin, D. M. Spasyuk, R. A. Lalancette and D. E. Prokopchuk, *J Am Chem Soc*, 2022, **144**, 12632.
3. H. A. Spinney, C. R. Clough and C. C. Cummins, *Dalton Trans*, 2015, **44**, 6784.
4. G. R. Fulmer, A. J. M. Miller, N. H. Sherden, H. E. Gottlieb, A. Nudelman, B. M. Stoltz, J. E. Bercaw and K. I. Goldberg, *Organometallics*, 2010, **29**, 2176.
5. S. Stoll and A. Schweiger, *J. Magn. Reson.*, 2006, **178**, 42.
6. F. Neese, *WIREs Comput. Mol. Sci.*, 2022, **12**, e1606.
7. F. Weigend and R. Ahlrichs, *Phys. Chem. Chem. Phys.*, 2005, **7**, 3297.
8. F. Weigend, *Phys. Chem. Chem. Phys.*, 2006, **8**, 1057.
9. Y. Zhao and D. G. Truhlar, *J. Phys. Chem. A*, 2005, **109**, 5656.
10. C. Kollmar, K. Sivalingam, B. Helmich-Paris, C. Angeli and F. Neese, *J. Comput. Chem.*, 2019, **40**, 1463.
11. F. Weigend, *J. Comput. Chem.*, 2008, **29**, 167.
12. S. Grimme, J. Antony, S. Ehrlich and H. Krieg, *J. Chem. Phys.*, 2010, **132**, 154104.
13. S. Grimme, S. Ehrlich and L. Goerigk, *J. Comput. Chem.*, 2011, **32**, 1456.
14. A. V. Marenich, C. J. Cramer and D. G. Truhlar, *J. Phys. Chem. B*, 2009, **113**, 6378.

15. V. Ásgeirsson, B. O. Birgisson, R. Bjornsson, U. Becker, F. Neese, C. Riplinger and H. Jónsson, *J. Chem. Theory Comput.*, 2021, **17**, 4929.